

THE MORPHOLOGICAL DEPENDENT TULLY-FISHER RELATION OF SPIRAL GALAXIES

SHIYIN SHEN^{1,3}, CAIHONG WANG^{1,2}, RUIXIANG CHANG^{1,3}, ZHENGYI SHAO^{1,3}, JINLIANG HOU^{1,3}, CHENGGANG SHU³

¹ Key Laboratory for Research in Galaxies and Cosmology, Shanghai Astronomical Observatory, Chinese Academy of Sciences, 80 Nandan Road, Shanghai, 200030, China

² Graduate University of Chinese Academy of Sciences and

³ Key Lab for Astrophysics, Shanghai 200234

Draft version November 12, 2018

ABSTRACT

The Tully-Fisher relation of spiral galaxies shows notable dependence on morphological types, with earlier type spirals having systematically lower luminosity at fixed maximum rotation velocity V_{\max} . This decrement of luminosity is more significant in shorter wavelengths. By modeling the rotation curve and stellar population of different morphological type spiral galaxies in combination, we find the V_{\max} of spiral galaxies is weakly dependent on the morphological type, whereas the difference of the stellar population originating from the bulge disk composition effect mainly account for the morphological type dependence of the Tully-Fisher relation.

Subject headings: galaxies: spiral - galaxies: stellar content - galaxies: kinematics and dynamics

1. INTRODUCTION

The Tully-Fisher relation (Tully & Fisher 1977, hereafter TFR) is an empirical relation between the absolute magnitude M and the maximum rotation velocity V_{\max} of spiral galaxies, which is typically expressed as

$$M = \alpha \text{Log} \left(\frac{V_{\max}}{200 \text{ km s}^{-1}} \right) + \beta, \quad (1)$$

where the values of slope α and zero-point β are dependent on the photometric band of the M being measured.

It has long been known that the TFR has a morphological type dependence, with earlier type spirals having systematically lower luminosity at fixed V_{\max} (Roberts 1978; Rubin et al. 1980). This luminosity difference is also waveband dependent, with larger offsets in shorter wavelengths. For example, in I band, Giovanelli et al. (1997) found a 0.32 mag lower zero-point of the TFR for Sa/Sab galaxies and 0.10 mag lower for Sb galaxies than the Sbc and later type spirals. In B band, Russell (2004) found that Sb galaxies have a zero-point of 0.57 mag lower than Sc galaxies. In a recent study, Russell (2008) compared the TFR-derived distances of nearby groups and clusters and found a mean difference of 0.19 mag in H band between the Sb and Sc spiral galaxies. Moreover, using a large sample of spiral galaxies, Masters et al. (2006, 2008) found that the morphological dependence of the TFR is not only a shift of the zero-point, but even dependent on the luminosity in the way that the differences are more pronounced for more luminous galaxies.

The morphological dependence of the TFR originates from either the differences of the stellar population (M) or the disk dynamics (V_{\max}) or both.

On one hand, it is well known that the colors of earlier type spirals are redder. Devereux & Young (1991) interpreted this color difference as originating from the bulge disk composition effect. The stellar population of bulges are typically older and more metal rich than that of the disks. A larger fraction of the bulge component in

earlier type spirals naturally results in a redder color on average for the whole galaxy. However, with a bulge disk decomposed sample, Kennicutt et al. (1994) studied and compared the star formation histories of only the disk component of different type spirals and found that the stellar population of the disks of later type spiral is also on average younger.

On the other hand, although the rotation curves of spiral galaxies are proposed to follow a universal shape (Persic & Salucci 1991; Persic et al. 1996), there is evidence showing that the rotation curves of early type spirals rise more rapidly in the inner region than that of late types (Corradi & Capaccioli 1990; Noordermeer et al. 2007). Noordermeer & Verheijen (2007) show that the massive Sa galaxies lie better in the well-defined TFR when using the asymptotic rotation velocity V_{asympt} instead of V_{\max} , implying a dependence of V_{\max} on the morphological type.

On the theoretical side, the zero-point, slope and scatter of the observed TFR can all be well accommodated by the current disk formation model in the framework of the cold dark matter hierarchical cosmogonies (Dalcanton et al. 1997; Mo et al. 1998; Mo & Mao 2000; Pizagno et al. 2005). However, the morphological dependence of the TFRs has not been probed in these studies because the bulge component in these models is typically neglected. Another limitation of these models is that the stellar populations have not been tackled with a physical prescription, but with pre-determined mass-to-light ratios.

In this study, we aimed to model the dynamics and stellar population of different type spiral galaxies in combination and try to find out which factor is the main contributor to the morphological dependence of the TFR. In specific, we will follow the dynamical model of Mo, Mao & White (1998, hereafter MMW) and extend it to include a bulge component. For the stellar population, we will parameterize the star formation histories of the disks and bulges separately and then derive their mass-to-light ratios in different bands using the stellar population synthesis code (Bruzual & Charlot 2003).

This paper is organized as follows. In Section 2, we describe our dynamical model of the spiral galaxies, including the disk, bulge and dark halo components respectively. In Section 3, we study the stellar properties of the disks and bulges with parameterized star formation histories. We compare our model predictions with the observational data in Section 4. We make discussions on the uncertainties of our results in Section 5 and finally give a brief summary in Section 6.

2. DYNAMICAL MODEL OF SPIRAL GALAXIES

Our modeling of the dynamics of spiral galaxies follows and simplifies the disk formation model of MMW, but with more attention on the bulge contribution. The interested reader is referred to MMW for detail. Here we repeat the essentials related to our study. In this model, initially, the gas and dark matter are uniformly mixed in a virialized halo. As a result of dissipative and radiative cooling, the gas gradually cools down and settles into a disc structure due to the conservation of angular momentum.

We define that the stellar mass of the galaxy finally formed is M_* and the fraction of this mass to the initial halo mass M_h is $m_s \equiv M_*/M_h$. We express the bulge fraction of the formed galaxy being f_b , so that the masses of the bulge and disk are $M_b = f_b M_*$ and $M_d = (1 - f_b)M_*$ respectively.

The rotation curve of a spiral galaxy is contributed by three dynamical components: halo, bulge and disk. We show and discuss our assumptions on each term below.

2.1. halo

The N -body simulations show that the collapsed and virialized dark halos follow a universal density NFW profile (Navarro, Frenk, & White 1996),

$$\rho(r) = \frac{V_h^2}{4\pi G r^2} \frac{c}{[\ln(1+c) - c/(1+c)]} \frac{r/r_s}{(r/r_s + 1)^2}, \quad (2)$$

where r_s is a scale radius, G is the gravitational constant, V_h is the circular velocity and c is the concentration parameter. The concentration c is defined as $c \equiv r_{200}/r_s$, where r_{200} is the virial radius¹ of the halo. For a given cosmology, the virial radius r_{200} , halo mass M_h and circular velocity V_h are related by

$$r_{200} = \frac{V_h}{10H(z)}, \quad M_h = \frac{V_h^3}{10GH(z)}, \quad (3)$$

where $H(z)$ is the Hubble constant at redshift z .

In this study, we use the concordance Λ CDM cosmology model, with $H_0 = 70 \text{ km s}^{-1} \text{ Kpc}^{-1}$, $\Omega_0 = 0.3$, $\Omega_\Lambda = 0.7$ and baryon mass density $\Omega_B = 0.04$.

With the assembling of the baryons into disk and bulge, the gravitational effect from the bulge and disk changes the initial halo mass distribution through contraction. We follow MMW and use the adiabatic contraction assumption to analysis this effect (see MMW for detail).

For a halo with given circular velocity V_h , the concentration c is the only parameter to be quantified. At given redshift z , the concentration parameter c is mainly correlated with the mass of the halos (Navarro et al. 1996;

Bullock et al. 2001). We adopt a simple parametrization of the concentration c at redshift zero as that in Shen et al. (2002):

$$c = 8.5 \left(\frac{V_h}{100 \text{ km s}^{-1}} \right)^{-1/3} \quad (4)$$

2.2. bulge

We assume that the bulge component of spiral galaxies has a spherical mass distribution and the mass density profile $\rho_b(r)$ follows a *Hernquist* profile (Hernquist 1990), whose projection approximates the classical $R^{1/4}$ surface brightness profile of elliptical galaxies. The $\rho_b(r)$ is expressed as

$$\rho_b(r) = \frac{M_b}{2\pi} \frac{a}{r} \frac{1}{(r+a)^3}, \quad (5)$$

where M_b is the total bulge mass, a is the bulge scale radius, which is correlated with the effective(half-light) radius R_e in the way $R_e \approx 1.82a$ [Equ. 38 of Hernquist (1990)]. To establish the dynamics of a bulge with mass M_b , we need to know the scale radius a or effective radius R_e . We assume that the bulges follow the observed size-mass($R - M$) relation of elliptical galaxies (Shen et al. 2003),

$$R_e(\text{Kpc}) = 3.47 \times 10^{-5} \left(\frac{M_b}{M_\odot} \right)^{0.56}. \quad (6)$$

2.3. disk

The surface brightness profile of spiral disks typically follow an exponential profile. Here, we assume the disk surface mass density profile is also exponential,

$$\mu_d(r) = \mu_0 \exp(-r/R_d) \quad (7)$$

where μ_0 is the central surface mass density and R_d is the scale-length. μ_0 and R_d are related to the total mass of the disk M_d through $M_d = 2\pi\mu_0 R_d^2$.

Since the observed size of the disk in a spiral galaxy is affected by its central bulge, we do not take the observed $R - M$ relation of spiral galaxies as that in the model. Following MMW, we assume that the disk size R_d is determined by its initial angular momentum J , which can be parameterized by a spin parameter λ

$$\lambda = J|E|^{1/2} G^{-1} M^{-5/2}, \quad (8)$$

where E is the total energy of the halo. With reasonable assumptions that the specific angular momentum per particle of the baryons is the same as the dark matter and there is no angular momentum transfer among different components, the angular momentum of the disk finally formed is therefore $J_d = m_d J$. Here, m_d is the fraction of baryons settling into the disk and is equal to $m_s(1 - f_b)$. The scale-length of the disk R_d then equals

$$R_d = \frac{1}{\sqrt{2}} \lambda r_{200} f_c^{-0.5} f_R(\lambda, c, m_d) \quad (9)$$

where f_c is a factor coming from the halo density profile and only dependent on concentration c (see Equ. 23 of MMW), f_R is a factor coming from both the halo density profile and the gravitational effects of disk and bulge(see

¹ Here, r_{200} is the radius within which the mean mass density is 200 times the cosmic critical density ρ_{crit} .

Equ. 29 of MMW). It is shown that the size of spiral galaxies predicted from λ is in excellent agreement with the observations (Syer et al. 1999; Shen et al. 2003).

Numerical simulations have found that the spin parameter λ of the dark matter halo follows a log-normal distribution with median $\bar{\lambda} \sim 0.04$ and scatter $\sigma_{\ln\lambda} \sim 0.4$ and this distribution is quite independent of the cosmology and halo properties (Bett et al. 2007). For the purpose of simplicity, we do not consider the scatter of the angular momentum distribution and take the median value $\lambda = 0.04$ for all disks (see more discussions in Section 5.1).

2.4. rotation curve

With the mass distribution of the bulge, halo and disk components determined through the model parameters shown above, the rotation curve of a spiral galaxy can be determined by the sum in quadrature of contributions from these three terms:

$$V^2(r) = G \frac{M_{DM}(r) + M_b(r)}{r} + V_d^2(r). \quad (10)$$

During the calculation of the term V_d^2 contributed from the disk component, the flattened geometry needs to be taken into account (Binney & Tremaine 1987).

To fully determine the rotation curve of a given spiral galaxy with stellar mass M_* , we still need to know the relative proportions of these three components (bulge, disk and dark halo). This could be done by settling the two other parameters, i.e. the baryon fraction m_s and the bulge-disk-ratio B/D^2 . We set the baryon fraction m_s to be a function of the halo mass (in terms of circular velocity V_h) (Shen et al. 2003),

$$m_s = \frac{0.13}{1 + (V_h/150 \text{ km s}^{-1})^{-2}}. \quad (11)$$

This assumption is based on the consideration that gas outflow process in low mass halo is efficient, due to their shallow potential well, and a large fraction of baryons is blown out of the dark halo, while the baryon fraction of high mass halos gradually approach the cosmic baryon fraction $\Omega_B/\Omega_0 \approx 0.13$ (White & Frenk 1991). The bulge-disk-ratio B/D is taken to be 0.5/0.3/0.1 for model Sa/Sb/Sc galaxies respectively (Simien & de Vaucouleurs 1986).

We show three examples of resulting rotation curves for three morphological types (Sa/Sb/Sc) in Fig. 1. All three model galaxies are chosen to have the same circular velocity $V_h = 120 \text{ km s}^{-1}$ and thus the same stellar mass $M = 3 \times 10^{10} M_\odot$. For the earlier type spiral, as we can see from the figure, due to the larger bulge component, our model predicts a steeper increase of rotation velocity in the inner region, which brings on the appearance of V_{\max} at smaller radius, and a systematically larger V_{\max} .

However, the value of V_{\max} only weakly correlates with the model type. The V_{\max} of the Sa(Sb) spiral is only 1.5(1.0) percent higher than the corresponding Sc spiral. This is because the relatively smaller bulge fraction of the later type spiral is always compensated by its larger disk fraction (see the components of rotation curves in Fig. 1).

² $B/D \equiv f_b/(1 - f_b)$

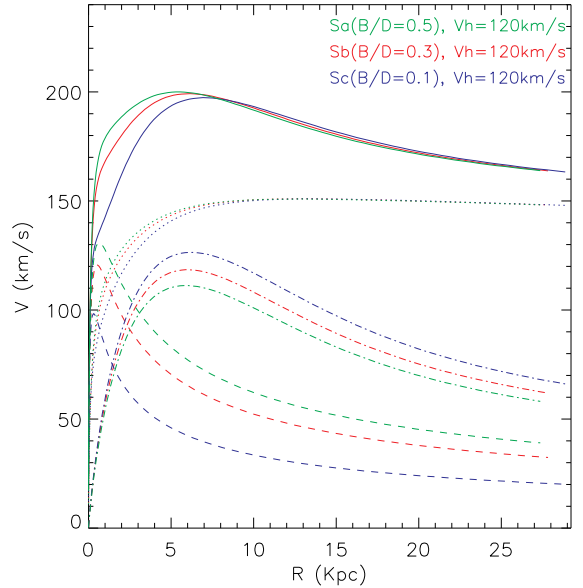


FIG. 1.— The rotation curves of the model galaxies with $V_h = 120 \text{ km s}^{-1}$. The solid lines show the rotation curve while the dot-dashed, dotted and dashed lines show the contributions from disk, halo and bulge components respectively. The green, red and blue lines represent the model Sa, Sb and Sc galaxies respectively.

3. STELLAR POPULATIONS OF SPIRAL GALAXIES

Besides the different dynamics, the bulge and disk also show different stellar populations. The bulges are typically old and show little recent star formation, while the star formation time-scales of the disks are long and there is still ongoing star formation throughout the disk at the present day.

In this study, we parameterize the stellar population of the bulge components with a single stellar population with age of 10G year(Gy). For the disks, following the usual convention, we parameterize their star formation histories(SFH) with an exponential function

$$SFR(t) \propto \exp(-t/\tau) \quad (12)$$

where τ is the time scale of the SFH. This simple analytical expression can parameterize different kinds of SFHs. For τ approaching 0, Equ. (12) represents a single stellar population. When τ tends to infinity, the star formation rate is a constant along the history. The age of the disks is also set to 10 Gy.

Kennicutt et al. (1994, hereafter K94) parameterized the SFH of the spiral disks with a b parameter, which is defined as

$$b \equiv \frac{SFR}{\langle SFR \rangle} \quad (13)$$

where SFR is the star formation rate today and $\langle SFR \rangle$ is the average star formation rate in past. They estimated the b parameter from UBV colors and $H\alpha$ fluxes for different morphological type spirals and found that the Sa/Sb/Sc disks have typical $b \approx 0.12/0.33/0.84$ and variation of about 0.05/0.15/0.20 respectively.³ With the SFHs parameterized by Equ. 12

³ The b values are taken from Table 4 of K94, where the subtypes include Sa/Sab/Sb/Sbc/Sc/Scd spirals. We average the b

as a prior, these b values correspond to the τ with median 3/5/30 Gy and 1σ range [2,4]/[4,7]/[10, ∞] Gy for Sa/Sb/Sc spirals respectively.⁴

Based on the SFHs assumed for disk and bulge components, we use the new version of the stellar population synthesis code of Bruzual & Charlot (2003), denoted as CB07, to calculate their mass-to-light ratios in different wavebands. The metallicity of the stellar population is set to be the solar value while the stellar initial mass function is taken from Chabrier (2003) with lower and upper mass limit being $0.1M_{\odot}$ and $100M_{\odot}$ respectively.

Finally, with the predetermined stellar mass m_s and B/D for each model galaxy, we calculate its absolute magnitudes in different optical wavebands.

4. MODEL PREDICTIONS

In this section, we show our model predicted morphologically dependent TFRs and compare them with the observational results. For each morphological type, we build 11 model galaxies with halo circular velocity V_h in the range from 100 to 200 km s^{-1} with an interval of 10 km s^{-1} . With the baryon fraction characterized by Equ. 11, the range of the stellar mass of our model galaxies is thus from 1.4×10^{10} to $2.3 \times 10^{11} M_{\odot}$.

In our model, there is only one free parameter, i.e. the disk star formation time scale τ in Equ. 12. We first set the τ values of different type spirals to be these suggested by K94, i.e. the median $\tau = 3/5/30$ Gy and its 1σ range being [2,4]/[4,7]/[10, ∞] Gy for Sa/Sb/Sc spirals respectively. We refer to this model setting as K94 model below.

4.1. I -band TFRs

Lots of recent observational TFR studies are in the near-infrared I band (e.g. Giovanelli et al. 1997; Dale et al. 1999; Vogt et al. 2004), which takes the advantage of better detector photometry than H band and less scatter in TFR than blue B band. More recently, Springob et al. (2007) compiled and published a new generation of a homogeneous galaxy catalog, referred to as the $SFI++$, which contains ~ 5000 spirals suitable for TFR study in I band. Based on the $SFI++$ catalog, the TFRs of Sa, Sb and Sc type spirals have been presented by Masters et al. (2006, hereafter M06). Here, we first show our model predicted I band TFRs for different type galaxies and make comparisons with the results of M06.

The K94 model predicted I band TFRs of Sc, Sb and Sa spirals are shown in the top left, top right and bottom left panels of Fig. 2 respectively. The model galaxies are represented by the triangles (Sc), squares (Sb) and stars (Sa) while the fitted TFRs are shown as the solid lines in each panel. The observed I band TFRs of different type spirals of M06 are shown as the dashed lines for comparison. The dotted lines in each panel show the ranges of model predicted TFRs when the disk star formation time scale τ varies in its 1σ range. Inside its

values of Sa and Sab sub-types as the Sa type. The b value of Sb type is kept. For Sc type, we average the b values of Sbc and Sc/Scd sub-types. The variations of b are estimated from Fig. 6 of K94.

⁴ Here, the 1σ range denotes the 32th to 68th percentiles of the τ distribution and is calculated from the estimated variation of b . For Sc spirals, during the calculation of the range of τ , we force the upper limit of b to be 1, corresponding to $\tau \sim \infty$, which gives the youngest average stellar population as that can do by Equ. 12.

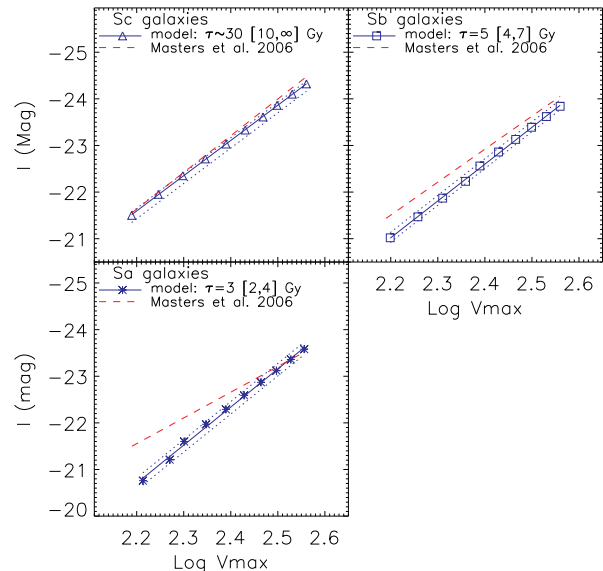


Fig. 2.— The model predicted I band TFRs of different morphological type spiral galaxies. The triangles, squares and stars represent the model Sc, Sb and Sa galaxies in top left, top right and bottom left panels respectively. The solid lines show the best TFR fittings of model galaxies while the observed TFRs of M06 are shown as the dashed lines for comparison. The dotted lines in each panel show the range of the model predicted TFRs when the star formation time scale τ varies in its 1σ range (as that denoted in the brackets).

range, a larger τ results a larger zero-point of the TFR, i.e. galaxies will be brighter at given V_{max} for larger τ .

Sc type spirals (include Sbc/Sc/Scd) are the dominant morphological type in TFR studies⁵. Lots of the TFR studies use Sc spirals as the reference and make morphological type corrections on other types, e.g. Giovanelli et al. (1997); Dale et al. (1999); Ziegler et al. (2002). For Sc spirals, as we can see, by setting the model parameters to be either the typical values from numerical simulations (e.g. λ and c) or being constrained from other observations (e.g. $\tau \sim 30$ Gy) without any further fine-tuning, our model predicted I band TFR is in excellent agreement with the observations.

However, with default settings of model parameters, our model predicted TFRs of Sb and Sa spirals are not well consistent with the observations of M06. The predicted TFR of Sb spirals ($\tau = 5$ Gy) have a systematically larger zero-point than observations, i.e. the model predicted luminosity is too bright. When τ reaches its upper range 7 Gy, the discrepancy becomes smaller, but still be far from consistent with observations. We will discuss this discrepancy in more detail in next section.

For Sa spirals, the slope of the observed TFR is significantly shallower than our model predictions. However, as that discussed in Giovanelli et al. (1997) and M06, the disagreement of the TFR slope of the Sa spirals should be interpreted in caution because the incompleteness of the Sa spirals is large, especially in the low luminosity end, which will artificially bias the slope to lower value. On the other hand, our modeling on the B/D of

⁵ The later type spirals are more likely to be strong HI or H α emitters so that the measurement of the rotation width is easier.

Sa spirals is a constant 0.5, which might be too simplified. In the study of M06, all the S0/Sa/Sab galaxies are grouped as Sa type. Among three sub-types, the earlier type galaxies, e.g. S0, having systematically larger B/D , are also systematically brighter. Therefore, from low V_{\max} to high V_{\max} galaxies, there is actually a systematical change of B/D , which will also shallow the slope of TFR. By introducing a systematical change of B/D as function of V_{\max} , we can in principle reproduce the slope of Sa spirals as observed. However, we prefer not to tune our model to reproduce this relation with a cost of introducing more uncertainties.

Comparing with the uncertainties in the modeling of the TFR slope, the zero-point is quite robust. Moreover, many studies of the morphological dependence of the TFRs only report a global shift of the zero-point, e.g. Giovanelli et al. (1997); Russell (2004, 2008) (see next section). Therefore, in the following section, we parameterize the morphological dependence of the TFRs only with the shift of the zero-point ΔM .

4.2. morphology dependent TFRs in different bands

We choose the zero-point shift ΔM of the TFRs at $V_{\max} = 200 \text{ km s}^{-1}$, where the corresponding absolute magnitude is roughly the M_* of the luminosity function of spiral galaxies and where the number counts of galaxies in a flux-limited sample normally peaks. In this case, $\Delta M = \Delta \beta$ of Equ. 1.

We show the ΔM between Sb and Sc spirals in the top panel of Fig. 3, whereas the ΔM between Sa and Sc spirals is shown in the bottom panel. The model predicted ΔM in different wavebands are connected as a function of their effective wavelengths with lines. The wavebands include U, B, V, R, I, J, H, K and the wavelength ranges from 0.33 to 2.2 micron. The observed difference of ΔM at $V_{\max} = 200 \text{ km s}^{-1}$ in different bands found in the literature are plotted against their effective wavelengths. Results from different authors are labeled with different symbol types. The references and details of these morphology dependent TFRs are listed in Table 1. A few other studies in the literature are not quoted in Table 1 and Fig. 3, including Rubin et al. (1985), Giovanelli et al. (1997) and the TFR of Sb spirals of Sandage (2000). Rubin et al. (1985) found the magnitude differences ΔM between Sa and Sc spirals are as high as 2 mag in B band and 1 mag in H band, whose number of each type galaxies is limited (< 20) and without error estimation quoted for the parameters of TFRs. The I band data of Giovanelli et al. (1997) has been expanded and re-analyzed by M06 and their results are generally consistent. The TFR of Sb spirals in Sandage (2000) is arbitrarily neglected, where its zero-point is even lower than Sc spirals, i.e. $\Delta M(\text{Sb-Sc}) < 0$, contradictory to most of the other studies.

The solid lines in Fig. 3 show predictions from the K94 model, i.e. the model with $\tau = 3, 5, 30 \text{ Gy}$ for Sa, Sb, Sc spirals respectively. The shadowed regions show the ranges of model predicted ΔM when τ varies in its 1σ range. As we can see, the K94 model over-predicts the differences of the zero-points significantly for both Sb/Sc and Sa/Sc pairs. The average observed zero-point differences in near-infrared bands are $\Delta M(\text{Sb-Sc}) \sim 0.15 \text{ mag}$ and $\Delta M(\text{Sa-Sc}) \sim 0.20 \text{ mag}$, whereas the model prediction is as high as $\Delta M(\text{Sb-Sc}) \sim 0.45 \text{ mag}$ and $\Delta M(\text{Sa-}$

Sc) $\sim 0.60 \text{ mag}$. That means, if the differences of the stellar populations of the disks of different type spirals are as that suggested by K94, the shift of the zero-point of the TFRs would be much larger than observed.

With the disk star formation time scale τ approaching its upper range (the lower boundary of the shadowed region), the discrepancy between the model predicted ΔM and the observations becomes smaller. This result prompts us to consider an extreme case, $\tau = 30 \text{ Gy}$ for both Sa and Sb disks. In this case, the stellar populations of the disks of different type spirals are the same, while the different global colors of different type spirals only originate from the bulge disk composition effect. This scenario is consistent with the results of Devereux & Young (1991). To distinguish it from the K94 model, we refer to this scenario ($\tau = 30 \text{ Gy}$ for all type disks) as the ‘composition’ model below.

For the ‘composition’ model, the model predicted ΔM as function of the effective wavelength is shown as the dotted lines in Fig. 3. Surprisingly, the predicted ΔM from this model, especially in near-infrared bands, is generally consistent with observations, either for Sb/Sc or Sa/Sc pairs. The predicted ΔM in B band is smaller than that observed. A possible solution to this discrepancy is the dust extinction which has not been taken into account in our model. If the face-on dust extinction of earlier type spirals is more significant, the ΔM in blue band will be larger than now we predicted (see detailed discussions in Section 5.3).

Finally, it is worth mentioning that the ΔM between different spiral types is not contributed by the stellar population alone but composed by both the dynamics and stellar population. As we have shown in section 2.4, for the galaxies with the same stellar mass $3 \times 10^{10} M_{\odot}$, the V_{\max} of a Sa(Sb) spiral is about 1.5(1.0) percent higher than Sc spiral, which corresponds to the $\Delta M \sim 0.04(0.03) \text{ mag}$, independent of the wavebands. This contribution is shown as two dashed horizontal lines in the top and bottom panels of Fig. 3. However, as we can see, the stellar population is still the dominant contributor to the morphological dependence of the TFR.

5. DISCUSSION

There are some uncertainties in our modeling of both dynamics and stellar population of the spiral galaxies, e.g. the scatters of model parameter, the diverse bulge properties and the internal dust extinction etc. We discuss these issues below.

5.1. scatters of model parameter

In our modeling, we only take the typical values for each model parameter and do not consider their scatters except the key parameter τ . However, all these model parameters show scatters as suggested by either numeric simulations or observations, e.g. Mo & Mao (2000); Jing (2000); Shen et al. (2002). If the scatters of model parameters are independent variables and do not correlate with the morphological types (as suggested in our model), these scatters will only make contributions to the scatters of the predicted TFRs and will not affect any of our conclusions (Mo & Mao 2000; Shen et al. 2002).

However, the morphological type may correlate with the spin value of a galaxy. A smaller λ may trigger a formation of larger bulge easier through disk instability

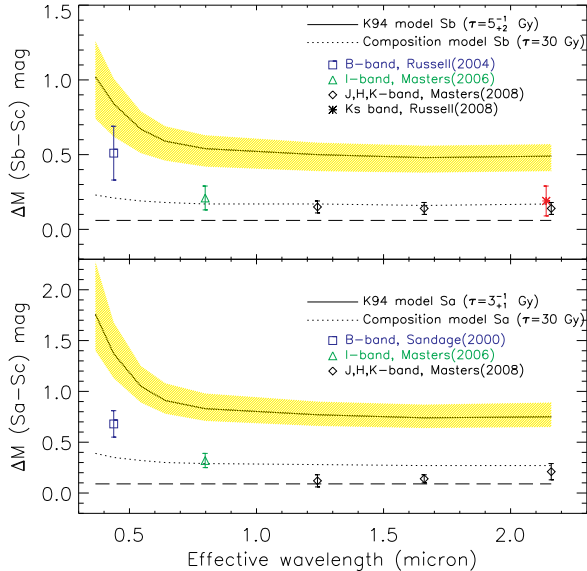


FIG. 3.— The morphology dependence of the TFR in different wavebands. The solid and dotted curves show the predicted shift of the zero-point of the TFRs, ΔM , as function of wavelength from the K94 model and ‘composition’ model respectively (see text). The dashed horizontal lines show the contributions to ΔM from the V_{\max} (see text). The upper panel shows ΔM between Sb and Sc spirals, while the ΔM between Sa and Sc is shown in the bottom panel. The observed ΔM in B, I, J, H and K band are labeled for comparison.

(Shen et al. 2003), so that induce an earlier type spiral. In other words, the earlier type spirals would be biased to the galaxies with systematically lower λ when we considered the scatter of λ . In this case, the resulted V_{\max} of earlier type spirals will be even larger because of the lower λ (Mo & Mao 2000) and thus the room left for the stellar population in ΔM is less.

5.2. pseudo and classical bulges

In this study, we have treated all the bulges as scaled elliptical, i.e. the classical bulges, for simplicity.

The current view on the bulges is quite complex. There are mainly two types of bulge, i.e. the classical bulge and the pseudo-bulge, which may be originated from different physical formation processes (Fisher & Drory 2008; Fisher et al. 2009; Gadotti 2009). The classical bulges are similar to scaled elliptical galaxies, with their surface brightness following classical $R^{1/4}$ profile and colors being red. The pseudo-bulges tend to show younger stellar population and their density profiles can be characterized by a Sérsic profile with Sérsic index n significantly smaller than 4. The classical bulges typically appear in earlier type spirals and their masses are high. The majority of the stellar mass of the bulges is in classical bulges [$\sim 90\%$, Gadotti (2009)].

If the bulges of late type (e.g. Sc) spirals are pseudo-bulges, the difference of stellar population between early and late type spirals will be even larger because the pseudo-bulges are bluer than classical bulges. This will increase the predicted ΔM between the early and late type spirals and decrease the allowed differences between their disks again.

5.3. dust extinction

In our modeling, we have not considered the effect of internal dust extinction, which might be different for different type spirals.

Fortunately, the internal dust extinction has at least been partly corrected in most of the observational TFR studies, e.g. Giovanelli et al. (1997); Masters et al. (2006, 2008). In these studies, they all made the corrections of the internal dust extinction using the parametrization of Giovanelli et al. (1994),

$$A = \gamma \text{Log}(a/b) \quad (14)$$

where γ is a waveband dependent coefficient and a/b is the observed axis ratio indicating the inclination angle of the spiral disk. This parametrization of the dust extinction has accounted the extinction from the geometry effect, i.e. it has corrected all the spiral disk to face-on viewing and assumed zero dust extinction for face-on case ($A \sim 0$ for $a/b \sim 1$).

However, the internal dust extinction of face-on spirals may not be negligible (Shao et al. 2007; Driver et al. 2007). The inner parts of the spiral disks are very likely to be optical thick even when viewed in face-on (Giovanelli et al. 1994). The dependence of this face-on extinction on the morphological type is complicate. On one hand, the later type spiral disks are gas richer and so that may contain more dust (Stevens et al. 2005). On the other hand, the earlier type spirals have larger bulge component and this component suffers more from the dust extinction because the dust layer is peaked in the central region (Tuffs et al. 2004; Driver et al. 2007). Counteracting these two effects, the global dust extinction may only be weakly dependent on the morphological types. A very recent study of Muñoz-Mateos et al. (2009) based on the multi-wavelength data shows that there is a weak global trend of the internal dust extinction, $Sb > Sa > Sc$.

If the face-on dust extinction of early type spirals were more significant considering their more concentrated light, the smaller ΔM predicted by the ‘composition’ model in B band could be explained since the extinction in B band is 5 times more larger than K band given the typical extinction curve of normal spiral galaxies (Shao et al. 2007). Moreover, if we took the higher dust extinction for the early type spirals into our model, the model predicted ΔM would be larger, thus the stellar populations of different type disks even could not be very different as that suggested by K94.

6. SUMMARY

In this paper, we have studied the morphological dependent TFRs by modeling the dynamics and stellar population of spiral galaxies in combination. We model the dynamics of spiral galaxies by following the disk formation model of MMW and extending it to include a bulge component. We parameterize the SFHs of the bulge and disk separately and derive their mass-to-light ratios with population synthesis code of Bruzual & Charlot (2003). Our model reproduces the observed I band TFR of the Sc spirals very well without any free parameters. Our model shows that the morphological dependence of the TFRs is mainly contributed by the stellar population through bulge disk composi-

tion effect, although the effect from the dynamics is not negligible.

The effects of the dynamics and stellar population on the morphological dependence of the TFR are different. The shift of the V_{\max} (or luminosity), caused by dynamics, shows a characteristic that is independent of the wavebands. On the other hand, the shift of the zero-point of TFR is a function of the wavebands, when the morphological dependence is caused by the stellar population. Therefore, the morphological dependence of the TFR in different bands is an effective way to constrain the dynamics and stellar populations of spiral galaxies. Our results show that the observed morphological depen-

dent TFRs are consistent with a scenario that the stellar population of different type spirals are only different in the bulge disk composition on average.

ACKNOWLEDGMENTS

We thank the anonymous referee for posing questions which significantly clarified the analysis in this paper. This project is supported by NSFC10803016, NSFC10833005, NKBRSF2007CB815402, Shanghai Rising-Star Program(08QA14077) and Shanghai Municipal Science and Technology Commission No. 04dz_05905.

REFERENCES

- Bett, P., Eke, V., Frenk, C. S., Jenkins, A., Helly, J., & Navarro, J. 2007, *MNRAS*, 376, 215
- Binney, J. & Tremaine, S. 1987, *Galactic dynamics*, ed. J. Binney & S. Tremaine
- Bruzual, G. & Charlot, S. 2003, *MNRAS*, 344, 1000
- Bullock, J. S., Kolatt, T. S., Sigad, Y., Somerville, R. S., Kravtsov, A. V., Klypin, A. A., Primack, J. R., & Dekel, A. 2001, *MNRAS*, 321, 559
- Chabrier, G. 2003, *PASP*, 115, 763
- Corradi, R. L. M. & Capaccioli, M. 1990, *A&A*, 237, 36
- Dalcanton, J. J., Spergel, D. N., & Summers, F. J. 1997, *ApJ*, 482, 659
- Dale, D. A., Giovanelli, R., Haynes, M. P., Hardy, E., & Campusano, L. E. 1999, *AJ*, 118, 1468
- Devereux, N. A. & Young, J. S. 1991, *ApJ*, 371, 515
- Driver, S. P., Popescu, C. C., Tuffs, R. J., Liske, J., Graham, A. W., Allen, P. D., & de Propris, R. 2007, *MNRAS*, 379, 1022
- Fisher, D. B. & Drory, N. 2008, *AJ*, 136, 773
- Fisher, D. B., Drory, N., & Fabricius, M. H. 2009, *ApJ*, 697, 630
- Gadotti, D. A. 2009, *MNRAS*, 393, 1531
- Giovanelli, R., Haynes, M. P., Herter, T., Vogt, N. P., da Costa, L. N., Freudling, W., Salzer, J. J., & Wegner, G. 1997, *AJ*, 113, 53
- Giovanelli, R., Haynes, M. P., Salzer, J. J., Wegner, G., da Costa, L. N., & Freudling, W. 1994, *AJ*, 107, 2036
- Hernquist, L. 1990, *ApJ*, 356, 359
- Jing, Y. P. 2000, *ApJ*, 535, 30
- Kennicutt, Jr., R. C., Tamblyn, P., & Congdon, C. E. 1994, *ApJ*, 435, 22
- Masters, K. L., Springob, C. M., Haynes, M. P., & Giovanelli, R. 2006, *ApJ*, 653, 861
- Masters, K. L., Springob, C. M., & Huchra, J. P. 2008, *AJ*, 135, 1738
- Mo, H. J. & Mao, S. 2000, *MNRAS*, 318, 163
- Mo, H. J., Mao, S., & White, S. D. M. 1998, *MNRAS*, 295, 319
- Muñoz-Mateos, J. C., Gil de Paz, A., Boissier, S., Zamorano, J., Dale, D. A., Pérez-González, P. G., Gallego, J., Madore, B. F., Bendo, G., Thornley, M. D., Draine, B. T., Boselli, A., Buat, V., Calzetti, D., Moustakas, J., & Kennicutt, R. C. 2009, *ApJ*, 701, 1965
- Navarro, J. F., Frenk, C. S., & White, S. D. M. 1996, *ApJ*, 462, 563
- Noordermeer, E., van der Hulst, J. M., Sancisi, R., Swaters, R. S., & van Albada, T. S. 2007, *MNRAS*, 376, 1513
- Noordermeer, E. & Verheijen, M. A. W. 2007, *MNRAS*, 381, 1463
- Persic, M. & Salucci, P. 1991, *ApJ*, 368, 60
- Persic, M., Salucci, P., & Stel, F. 1996, *MNRAS*, 281, 27
- Pizagno, J., Prada, F., Weinberg, D. H., Rix, H.-W., Harbeck, D., Grebel, E. K., Bell, E. F., Brinkmann, J., Holtzman, J., & West, A. 2005, *ApJ*, 633, 844
- Roberts, M. S. 1978, *AJ*, 83, 1026
- Rubin, V. C., Burstein, D., Ford, Jr., W. K., & Thonnard, N. 1985, *ApJ*, 289, 81
- Rubin, V. C., Burstein, D., & Thonnard, N. 1980, *ApJ*, 242, L149
- Russell, D. G. 2004, *ApJ*, 607, 241
- . 2008, *ArXiv e-prints*
- Sandage, A. 2000, *PASP*, 112, 504
- Shao, Z., Xiao, Q., Shen, S., Mo, H. J., Xia, X., & Deng, Z. 2007, *ApJ*, 659, 1159
- Shen, S., Mo, H. J., & Shu, C. 2002, *MNRAS*, 331, 259
- Shen, S., Mo, H. J., White, S. D. M., Blanton, M. R., Kauffmann, G., Voges, W., Brinkmann, J., & Csabai, I. 2003, *MNRAS*, 343, 978
- Simien, F. & de Vaucouleurs, G. 1986, *ApJ*, 302, 564
- Springob, C. M., Masters, K. L., Haynes, M. P., Giovanelli, R., & Marinoni, C. 2007, *ApJS*, 172, 599
- Stevens, J. A., Amure, M., & Gear, W. K. 2005, *MNRAS*, 357, 361
- Syer, D., Mao, S., & Mo, H. J. 1999, *MNRAS*, 305, 357
- Tuffs, R. J., Popescu, C. C., Völk, H. J., Kylafis, N. D., & Dopita, M. A. 2004, *A&A*, 419, 821
- Tully, R. B. & Fisher, J. R. 1977, *A&A*, 54, 661
- Vogt, N. P., Haynes, M. P., Herter, T., & Giovanelli, R. 2004, *AJ*, 127, 3273
- White, S. D. M. & Frenk, C. S. 1991, *ApJ*, 379, 52
- Ziegler, B. L., Böhm, A., Fricke, K. J., Jäger, K., Nicklas, H., Bender, R., Drory, N., Gabasch, A., Saglia, R. P., Seitz, S., Heidt, J., Mehlert, D., Möllenhoff, C., Noll, S., & Sutorius, E. 2002, *ApJ*, 564, L69

TABLE 1 The observed morphological dependent TFRs in literatures. All the TFRs are re-shaped in the form of Equ. (1). ΔM is the shift of the zero-point β relative to the Sc spirals in the same study.

Reference	Waveband	type	sub-type	a	b	ΔM
Sandage (2000), Table 13	B	Sa	Sa/Sab	-6.97	-20.46 ± 0.12	$0.68 \pm .13$
		Sc	Sbc/Sc/Scd	-6.97	-21.14 ± 0.06	0
Russell (2004) Equ. 2 and 3	B	Sb	Sab/Sb/Sbc/Sc II-IV	-5.24 ± 0.10	-20.42 ± 0.16	$0.51 \pm .18$
		Sc	Sbc/Sc I-II	-4.91 ± 0.20	-20.93 ± 0.09	0
Masters et al. (2006), Table 4	I	Sa	S0/Sa/Sab	-5.52 ± 0.40	-21.34 ± 0.07	0.32 ± 0.07
		Sb	Sb	-7.07 ± 0.17	-21.45 ± 0.03	0.21 ± 0.08
		Sc	Sbc/Sc/Scd	-7.87 ± 0.15	-21.66 ± 0.02	0
Masters et al. (2008), Table 2	J	Sa	S0/Sa/Sab	-6.09 ± 0.30	-21.84 ± 0.06	0.12 ± 0.06
		Sb	Sb/Sbc	-7.80 ± 0.19	-21.81 ± 0.03	0.15 ± 0.04
		Sc	Sc/Scd	-9.23 ± 0.20	-21.96 ± 0.02	0
	H	Sa	S0/Sa/Sab	-6.08 ± 0.27	-22.62 ± 0.05	0.16 ± 0.05
		Sb	Sb/Sbc	-7.80 ± 0.19	-22.64 ± 0.03	0.14 ± 0.04
		Sc	Sc/Scd	-9.17 ± 0.20	-23.78 ± 0.02	0
	K	Sa	S0/Sa/Sab	-6.95 ± 0.24	-22.85 ± 0.03	0.21 ± 0.04
		Sb	Sb/Sbc	-8.64 ± 0.17	-22.92 ± 0.02	0.14 ± 0.04
		Sc	Sc/Scd	-10.09 ± 0.18	-23.06 ± 0.02	0
Russell (2008)	K_s	Sb	Sa/Sab/Sb	–	–	0.19 ± 0.10